**Supplementary Information**

# Magnetic ordering in an $(Fe_{0.2}Cr_{0.8})_{1.5}[Cr(CN)_6]$ Prussian blue analogue studied with synchrotron radiation based spectroscopies

Francisco Jesús Luque,[a] Iwona Agnieszka Kowalik,[b] Juan Pablo Prieto-Ruiz,[c] Miguel Ángel Niño,[d] Helena Prima-García,[c] Francisco Manuel Romero,[c] Dimitri Arvanitis,[e] Eugenio Coronado,[c] Rodolfo Miranda,[a,d,f] and Juan José de Miguel*[a,f,g]

[a] Departamento de Física de la Materia Condensada, Universidad Autónoma de Madrid, Cantoblanco, 28049-Madrid, Spain.

[b] Institute of Physics, Polish Academy of Sciences, 02668-Warsaw, Poland.

[c] Instituto de Ciencia Molecular (ICMol), Universitat de València, 46980-Paterna, Spain.

[d] IMDEA-Nanoscience, Cantoblanco, 28049 Madrid, Spain.

[e] Department of Physics and Astronomy, Uppsala University, 75237-Uppsala, Sweden.

[f] Condensed Matter Physics Centre (IFIMAC), Universidad Autónoma de Madrid, Cantoblanco, 28049 Madrid, Spain.

[g] Instituto de Física de Materiales "Nicolás Cabrera", Universidad Autónoma de Madrid, Cantoblanco, 28049 Madrid, Spain.

## 1 Sample preparation

The $(Fe_{0.2}Cr_{0.8})_{1.5}[Cr(CN)_6]\cdot 15\ H_2O$ Prussian blue analogue (PBA) films studied in this work were electrodeposited on a $5\times 10$ mm$^2$ Mylar substrate coated with 100 nm of Au using an aqueous solution (20 mL) containing $K_3[Cr(CN)_6]$ (5 mM), $CrCl_3$ (6.7 mM) and $FeCl_3$ (1.1 mM).[1,2] The chemicals were purchased from Sigma-Aldrich and used without further purification. The films were grown at a fixed potential E = −0.8 V versus a Ag/AgCl reference electrode. A Pt wire was used as a counter electrode. A Metrohm AUTOLAB potentiostat in coulometry mode was employed for the deposition. After preparation, films were rinsed with mili-Q water and dried at room temperature. The thickness of the grown films is controlled through the electrodeposition time, both magnitudes are found to follow a nearly linear relationship as previously observed for the $Cr_{5.5}(CN)_{12}\cdot 11.5\ H_2O$ compound.[3]. For the samples used in the XAS experiments described in the main manuscript a short electrodeposition pulse of 5 seconds was used, whereas 100 seconds of deposition time were used for the EXAFS samples. The deposited thicknesses were cross-checked after preparation with the help of an Ambios Technology XP-1 profilometer placed on a vibration isolation table. The compositional and morphological parameters of the thicker films are summarized in Table S.I.

### 1.1 Determination of the sample composition

The compositional factor $x$ is mainly established by the mixing ratio $Fe^{II}/(Fe^{II}+Cr^{II})$ of metal ions in the solution, but it is also dependent on the electrochemical potential used during the synthesis. After growth the value of $x$ was determined precisely by means of EDX (Energy Dispersive X ray) analysis yielding an Fe/Cr ratio of 1.53, in good agreement with the expected value of 1.5. These measurements were carried out on a Philips XL30 scanning electron microscope equipped with an EDAX DX4 microprobe. No presence of potassium in the structure of the material was detected.

The compound's stoichiometry can also be cross-checked with the help of infrared absorption spectroscopy. Attenuated total reflectance infrared (ATR-IR) spectra of the FeCrCr films were recorded on a Nicolet 5700 FT-IR spectrometer using a Veemax II Specular Reflectance Accessory. The IR-ATR spectra of the two films depicted in

**Table S.I** Compositional and morphological parameters of thin films of FeCrCr.

| Deposition time [s] | Thickness [nm] | x | Average particle size [nm] | RMS roughness [nm] |
|---|---|---|---|---|
| 1000 | 7000±200 | 0.3 | 1100±100 | 121 |
| 100 | 800±100 | 0.21 | 910±90 | 45 |

Figure S.1, of 800 nm and 7000 nm thickness, exhibit a principal band located around 2181 $cm^{-1}$ that is assigned to the cyanide stretching vibration of the $[Cr^{III}(CN)_6]^{3-}$ anion. Its position is known to vary in a nearly linear fashion along the $(Fe^{II}_xCr^{II}_{1-x})_3[Cr^{III}(CN)_6]_2 \cdot z\ H_2O$ series from 2186 $cm^{-1}$ ($x = 0$) to 2161 $cm^{-1}$ ($x = 1$).[1,3,4] Thus, the observed band corresponds to an iron molar fraction $x = 0.24 \pm 0.05$ in good agreement with the EDX analysis. As expected, the intensity of this band increases proportionally to the film thickness.

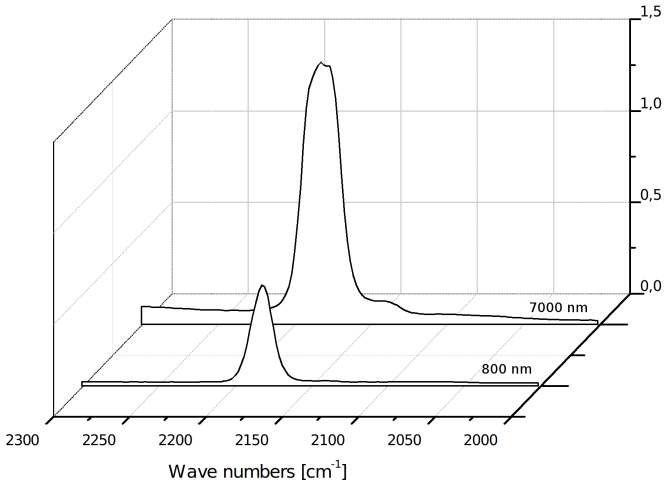


**Fig. S.1** IR spectra of the thin films synthesized with different thicknesses: 800 and 7000 nm.

The content of water in the structure was found by thermogravimetric measurements: in the low temperature range a first step centred at around 200°C, corresponding to desorption of surface and coordinated water molecules, supposed a weight loss of 32%. This could be translated to the presence of 15 water molecules in the PBA structure.

### 1.2 Surface morphology

The films' surface roughness and grain sizes were characterized with a Nanoscope Multimode (Veeco) atomic force microscope operating in tapping mode. RMS roughness and average particle size were analysed by using WSxM4 4.0 Develop 13.0 software[5] developed by Nanotec Electronics S.L.

One representative image for each film is presented in Figure S.2: they were acquired in tapping mode, with a $10\times10\ \mu m^2$ scan size. A polycrystalline structure can be observed, composed of pyramidal particles of different sizes. This type of morphology has been observed in the epitaxial electrodeposition of PBAs on a single-crystal Au(110) surface.[6] The average lateral particle size increases from 410 nm for the thinner (800 nm) film to 1070 nm for the thicker one. The rms film roughness also increases from 41 nm for the thinner sample to 121 nm for the thicker one. The increase of both particle size and roughness with deposition time and film thickness is consistent with a seeding growth mechanism as previously discussed for the electrosynthesis of thin films of $Cr_{5.5}(CN)_{12} \cdot 11.5\ H_2O$.[3,7]

## 2 Additional magnetic measurements

The hysteresis loops measured with SQUID magnetometry at 2 K for both films are presented in Figure S.3. They show a steep rise at a field of 0.5 T, followed by a slower increase up to 5 T. The films behave as soft magnets with similar coercivities, $H_c = 100$ mT. The remanent magnetization is $M_r = 0.71\ \mu_B$ for the thicker film and 0.35 $\mu_B$ for

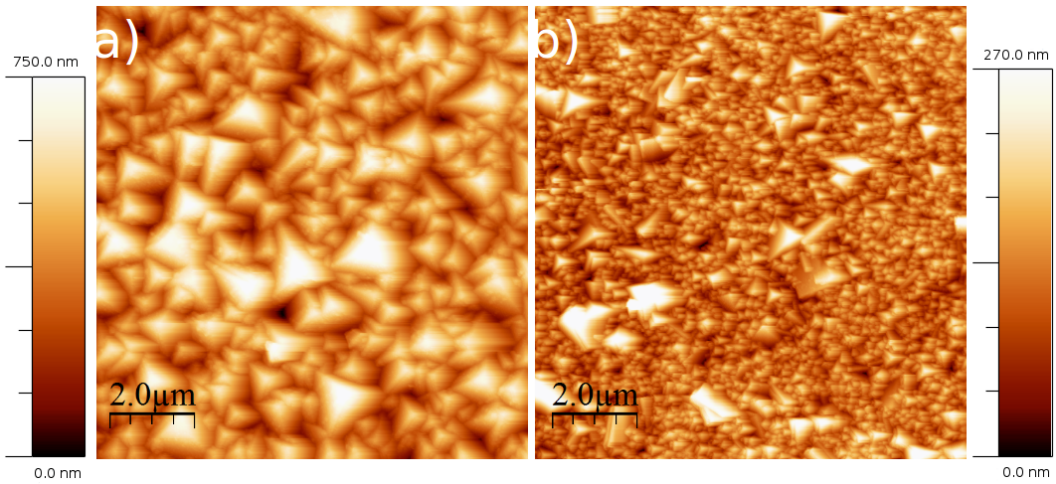


**Fig. S.2** AFM images of the surface topography of the FeCrCr films of (a) 7000 nm and (b) 800 nm thickness.

the thinner one, both of them far from saturation.

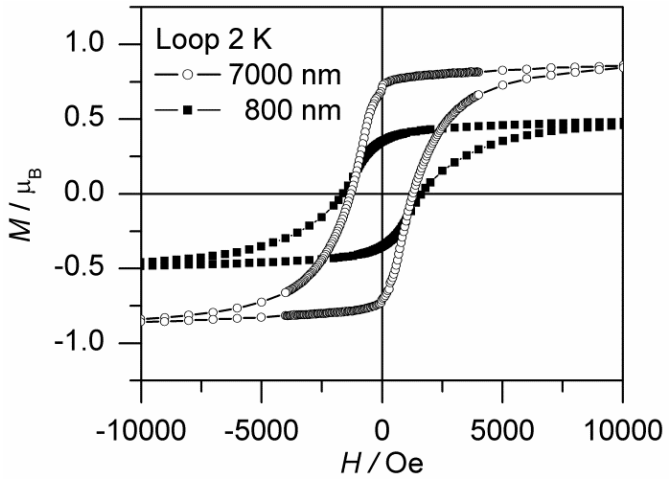


**Fig. S.3** Hysteresis loops measured with SQUID at T = 2 K for FeCrCr films of 800 nm and 7000 nm thickness.

Figure S.4 shows a fit to the reciprocal susceptibility data of the 7000 nm thick film with a Curie-Weiss law in the 240-340 K range, yielding $C = 5.57$ emu·K/mol and $\theta = -290$ K. The negative value of $\theta$ and the reduced value of the Curie constant $C$ indicate that antiferromagnetic short-range interactions dominate in the film even at 300 K.

Magneto-optic Kerr effect (MOKE) measurements were also carried out at ICMol. As an example, Figure S.5 depicts the hysteresis loops obtained at 170 K for the two FeCrCr films of 800 and 7000 nm thickness. The temperature evolution of the coercive field displayed in Fig. 9b of the main paper was determined from this type of curves.

## 3 Ligand Field parameters

We list here the complete sets of parameters used to analyse the XAS spectra presented in the paper. The fits have been performed using the CTM4XAS software;[8,9] this program is based on the TT-Multiplet code developed by Thole and Ogasawara.[10,11] These parameters can be divided into three different groups.

- *Atomic multiplet parameters:*
  - $\kappa$, the Slater-Condon parameter or percentage of reduction of the Slater integrals. Measures the covalency of the interaction between the metal and the ligand, with low values of $\kappa$ corresponding to covalent bonds.

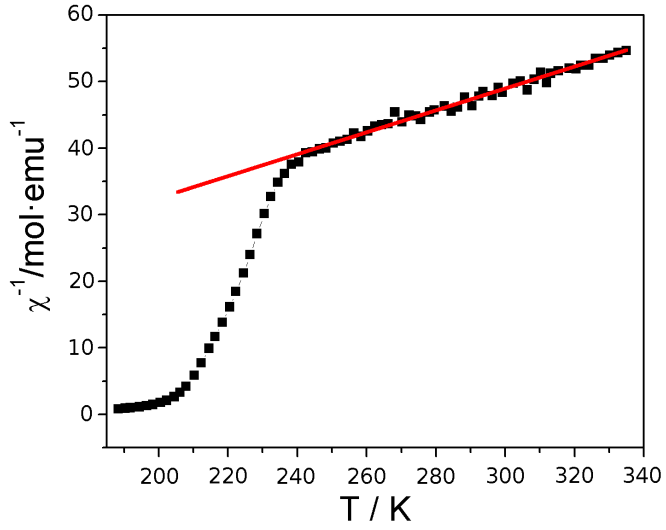


**Fig. S.4** Fit to the reciprocal susceptibility of the 7000 nm thick film with a Curie-Weiss law. The results of this fit reveal a predominance of antiferromagnetic interactions.

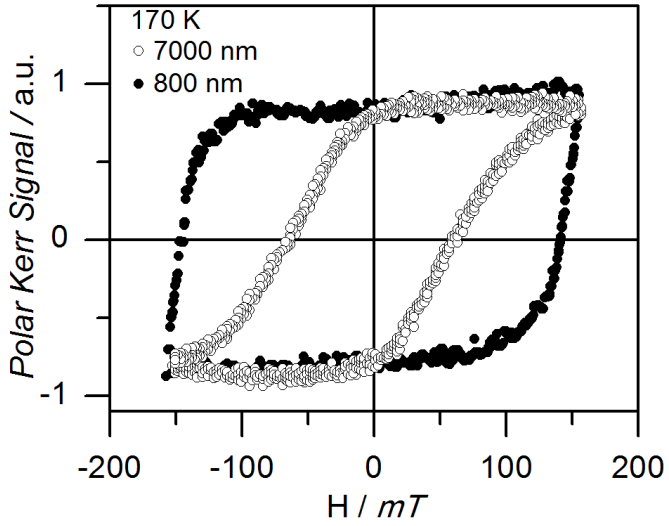


**Fig. S.5** Normalized MOKE hysteresis loops obtained at 170 K in polar configuration for the two FeCrCr films of 800 and 7000 nm thickness.

- $\zeta_{2p}$, the magnitude of the spin-orbit coupling (SOC) for the $2p$ orbitals. This parameter controls the energy separation between the $L_2$ and $L_3$ edges.
- $\zeta_{3d}$, SOC for the $3d$ orbitals. Although weak (of the order of $10^{-2}$ eV), it can have significant effects because it controls whether Hund's third rule is applicable or not in the ground state.

- *Crystal field parameters:*

  The crystal field splitting $10Dq$ represents the splitting between the $e_g$ and $t_{2g}$ sub-bands in octahedral symmetry. When the symmetry is reduced, these levels can be split further, with energy separations controlled by the parameters $D_t$ and $D_s$.

- *Charge transfer parameters:*

  The hybridization between the metal centre and the surrounding ligands is accounted for by considering the interaction between two or more electronic configurations.

– $EG$ ($EF$) gives the difference in energy of both configurations in the ground (excited) state.

– In octahedral symmetry, the hopping integrals $T_{e_g}$ and $T_{t_{2g}}$ control the mixing of the electronic states of the different configurations, giving rise to the formation of $\sigma$ or $\pi$-type bonds, respectively.

– If the symmetry is reduced the hopping integrals are denoted $T_{b_1}$, $T_{a_1}$, $T_{b_2}$, and $T_e$.

**Table S.II** Set of Ligand Field parameters for $Fe^{II}$ HS used with the CTM4XAS[9] software package to fit the experimental XAS spectra.

| | | 90° incidence −300 V bias | | 90° incidence no bias | 45° incidence no bias |
|---|---|---|---|---|---|
| | | 300 K | 150 K | 150 K | 150 K |
| | $\kappa$ (%) | 100 | 100 | 100 | 90 |
| | $\zeta_{2p}$ (eV) | 7.79 | 7.79 | 7.79 | 8.36 |
| | $\zeta_{3d}$ (eV) | 0.000 | 0.000 | 0.000 | 0.054 |
| | $10Dq$ (eV) | 0.8 | 0.9 | 0.8 | 1.5 |
| | $D_t$ (eV) | 0.040 | 0.025 | 0.025 | 0.151 |
| | $D_s$ (eV) | 0.070 | 0.012 | 0.002 | −0.254 |
| LMCT | $EG2$ | 0.0 | 0.0 | 0.0 | 1.0 |
| | $EF2$ | 0.0 | 0.0 | 0.0 | −0.4 |
| | $T_{b_1}$ | 0.0 | 0.0 | 0.0 | 1.5 |
| | $T_{a_1}$ | 0.0 | 0.0 | 0.0 | 2.0 |
| | $T_{b_2}$ | 0.0 | 0.0 | 0.0 | 0.8 |
| | $T_e$ | 0.0 | 0.0 | 0.0 | 0.8 |
| MLCT | $EG2$ | 1.5 | 1.7 | 5.5 | 0.0 |
| | $EF2$ | 0.5 | 0.8 | 4.0 | 0.0 |
| | $T_{b_1}$ | 2.8 | 3.1 | 1.9 | 0.0 |
| | $T_{a_1}$ | 2.5 | 3.1 | 1.9 | 0.0 |
| | $T_{b_2}$ | 3.8 | 3.4 | 2.5 | 0.0 |
| | $T_e$ | 3.4 | 3.5 | 2.6 | 0.0 |
| Configuration | % $\|3d^5\mathrm{L}^-\rangle$ | 48 | 47 | 29 | 0 |
| | % $\|3d^6\rangle$ | 52 | 53 | 71 | 74 |
| | % $\|3d^7\underline{\mathrm{L}}\rangle$ | 0 | 0 | 0 | 26 |
| # holes | | 4.48 | 4.47 | 4.29 | 3.74 |

**Table S.III** Set of Ligand Field parameters for $Fe^{II}$ LS.

| | | 90° incidence −300 V bias | | 90° incidence no bias | 45° incidence no bias |
|---|---|---|---|---|---|
| | | 300 K | 150 K | 150 K | 150 K |
| | $\kappa$ (%) | 50 | 50 | 60 | 60 |
| | $\zeta_{2p}$ (eV) | 8.20 | 8.20 | 8.20 | 8.36 |
| | $\zeta_{3d}$ (eV) | 0.067 | 0.067 | 0.067 | 0.054 |
| | $10Dq$ (eV) | 2.3 | 2.5 | 3.0 | 3.0 |
| | $D_t$ (eV) | 0.000 | 0.000 | 0.000 | 0.000 |
| | $D_s$ (eV) | 0.000 | 0.000 | 0.000 | 0.000 |
| LMCT | $EG2$ | 3.0 | 2.3 | 0.0 | 6.0 |
| | $EF2$ | 2.0 | 1.3 | 0.0 | 5.0 |
| | $T_{b_1}$ | 1.1 | 1.1 | 0.0 | 0.5 |
| | $T_{a_1}$ | 1.1 | 1.1 | 0.0 | 0.5 |
| | $T_{b_2}$ | 1.8 | 1.8 | 0.0 | 0.0 |
| | $T_e$ | 1.8 | 1.8 | 0.0 | 0.0 |
| MLCT | $EG2$ | 0.0 | 0.0 | 2.5 | 0.0 |
| | $EF2$ | 0.0 | 0.0 | 1.5 | 0.0 |
| | $T_{b_1}$ | 0.0 | 0.0 | 1.1 | 0.0 |
| | $T_{a_1}$ | 0.0 | 0.0 | 1.1 | 0.0 |
| | $T_{b_2}$ | 0.0 | 0.0 | 1.8 | 0.0 |
| | $T_e$ | 0.0 | 0.0 | 1.8 | 0.0 |
| Configuration | % $\lvert 3d^5\mathrm{L}^-\rangle$ | 30 | 33 | 31 | 0 |
| | % $\lvert 3d^6\rangle$ | 70 | 67 | 69 | 98 |
| | % $\lvert 3d^7\underline{\mathrm{L}}\rangle$ | 0 | 0 | 0 | 2 |
| # holes | | 4.30 | 4.33 | 4.31 | 3.98 |

**Table S.IV** Ligand Field parameters for $Fe^{III}$.

| | | 90° incidence −300 V bias | | 90° incidence no bias | 45° incidence no bias |
|---|---|---|---|---|---|
| | | 300 K | 150 K | 150 K | 150 K |
| | $\kappa$ (%) | 80 | 80 | 80 | 80 |
| | $\zeta_{2p}$ (eV) | 7.79 | 7.79 | 7.79 | 8.04 |
| | $\zeta_{3d}$ (eV) | 0.064 | 0.064 | 0.070 | 0.057 |
| | $10Dq$ (eV) | 1.1 | 1.3 | 1.4 | 1.3 |
| | $D_t$ (eV) | 0.000 | 0.000 | 0.000 | −0.020 |
| | $D_s$ (eV) | 0.000 | 0.000 | 0.000 | 0.150 |
| LMCT | $EG2$ | 0.9 | 0.5 | 0.7 | 2.5 |
| | $EF2$ | 0.0 | 0.0 | 0.0 | 1.5 |
| | $T_{b_1}$ | 0.8 | 0.8 | 0.9 | 1.5 |
| | $T_{a_1}$ | 0.8 | 0.8 | 0.9 | 1.5 |
| | $T_{b_2}$ | 1.0 | 1.0 | 1.0 | 0.5 |
| | $T_e$ | 1.0 | 1.0 | 1.0 | 0.9 |
| MLCT | $EG3$ | 0.9 | 0.9 | 2.0 | 0.0 |
| | $EF3$ | 2.5 | 2.5 | 3.2 | 0.0 |
| | $T_{b_1}$ | 1.7 | 1.6 | 1.2 | 0.0 |
| | $T_{a_1}$ | 1.7 | 1.6 | 1.3 | 0.0 |
| | $T_{b_2}$ | 0.6 | 0.7 | 1.0 | 0.0 |
| | $T_e$ | 0.6 | 0.7 | 1.0 | 0.0 |
| Configuration | % $\lvert 3d^4\mathrm{L}^-\rangle$ | 29 | 25 | 20 | 0 |
| | % $\lvert 3d^5\rangle$ | 56 | 60 | 65 | 85 |
| | % $\lvert 3d^6\underline{\mathrm{L}}\rangle$ | 15 | 15 | 15 | 15 |
| # holes | | 5.15 | 5.10 | 5.05 | 4.85 |

**Table S.V** Ligand Field parameters for $Cr^{II}$ HS.

| | | 90° incidence 300 V bias | | 90° incidence no bias | 45° incidence no bias |
|---|---|---|---|---|---|
| | | 300 K | 150 K | 150 K | 150 K |
| | $\kappa$ (%) | 80 | 80 | 80 | 80 |
| | $\zeta_{2p}$ (eV) | 5.78 | 5.78 | 5.78 | 5.78 |
| | $\zeta_{3d}$ (eV) | 0.042 | 0.042 | 0.042 | 0.032 |
| | $10Dq$ (eV) | 0.7 | 1.1 | 0.9 | 0.9 |
| | $D_t$ (eV) | 0.020 | 0.100 | 0.040 | −0.020 |
| | $D_s$ (eV) | −0.140 | −0.050 | −0.124 | −0.180 |
| LMCT | $EG3$ | 6.0 | 2.5 | 5.5 | 3.5 |
| | $EF3$ | 6.5 | 3.0 | 6.0 | 4.5 |
| | $T_{b_1}$ | 1.4 | 1.2 | 1.6 | 1.0 |
| | $T_{a_1}$ | 1.4 | 1.2 | 1.6 | 1.0 |
| | $T_{b_2}$ | 0.7 | 0.6 | 0.8 | 0.5 |
| | $T_e$ | 0.7 | 0.6 | 0.8 | 0.5 |
| MLCT | $EG2$ | −0.6 | −2.1 | −1.3 | −3.5 |
| | $EF2$ | −2.6 | −4.1 | −2.3 | −4.7 |
| | $T_{b_1}$ | 1.6 | 1.1 | 1.2 | 2.0 |
| | $T_{a_1}$ | 1.6 | 1.9 | 1.3 | 1.5 |
| | $T_{b_2}$ | 0.4 | 0.5 | 1.0 | 0.5 |
| | $T_e$ | 0.4 | 0.5 | 1.0 | 0.5 |
| Configuration | % $\|3d^3\mathrm{L}^-\rangle$ | 24 | 17 | 17 | 14 |
| | % $\|3d^4\rangle$ | 70 | 75 | 76 | 83 |
| | % $\|3d^5\underline{\mathrm{L}}\rangle$ | 6 | 8 | 7 | 3 |
| # holes | | 6.18 | 6.08 | 6.10 | 6.10 |

**Table S.VI** Ligand Field parameters for $Cr^{III}$.

| | | 90° incidence 300 V bias | | 90° incidence no bias | 45° incidence no bias |
|---|---|---|---|---|---|
| | | 300 K | 150 K | 150 K | 150 K |
| | $\kappa$ (%) | 70 | 80 | 70 | 70 |
| | $\zeta_{2p}$ (eV) | 5.78 | 5.78 | 5.78 | 5.78 |
| | $\zeta_{3d}$ (eV) | 0.000 | 0.000 | 0.048 | 0.048 |
| | $10Dq$ (eV) | 2.7 | 2.4 | 2.6 | 3.1 |
| | $D_t$ (eV) | −0.020 | −0.060 | −0.040 | 0.016 |
| | $D_s$ (eV) | 0.120 | 0.120 | 0.080 | 0.043 |
| LMCT | $EG2$ | −4.2 | −4.3 | −5.0 | −4.9 |
| | $EF2$ | −6.0 | −6.0 | −6.0 | −6.0 |
| | $T_{b_1}$ | 0.5 | 0.5 | 0.6 | 0.5 |
| | $T_{a_1}$ | 0.5 | 0.5 | 0.6 | 0.5 |
| | $T_{b_2}$ | 0.2 | 0.2 | 0.3 | 0.2 |
| | $T_e$ | 0.2 | 0.2 | 0.3 | 0.2 |
| MLCT | $EG3$ | −2.5 | −2.5 | −2.5 | −2.5 |
| | $EF3$ | −1.5 | −1.5 | −1.5 | −1.5 |
| | $T_{b_1}$ | 0.6 | 1.1 | 0.6 | 0.8 |
| | $T_{a_1}$ | 0.6 | 1.0 | 0.6 | 0.6 |
| | $T_{b_2}$ | 1.3 | 1.8 | 1.4 | 1.4 |
| | $T_e$ | 0.9 | 1.6 | 0.8 | 0.9 |
| Configuration | % $\|3d^2\mathrm{L}^-\rangle$ | 15 | 22 | 11 | 11 |
| | % $\|3d^3\rangle$ | 83 | 76 | 86 | 87 |
| | % $\|3d^4\underline{\mathrm{L}}\rangle$ | 2 | 2 | 3 | 2 |
| # holes | | 7.13 | 7.20 | 7.08 | 7.09 |

**Table S.VII** Ligand Field parameters for $Cr^{III}$ WCF.

| | | 90° incidence 300 V bias | | 90° incidence no bias | 45° incidence no bias |
|---|---|---|---|---|---|
| | | 300 K | 150 K | 150 K | 150 K |
| | $\kappa$ (%) | 90 | 90 | 90 | 80 |
| | $\zeta_{2p}$ (eV) | 5.67 | 5.67 | 5.67 | 5.66 |
| | $\zeta_{3d}$ (eV) | 0.047 | 0.047 | 0.047 | 0.037 |
| | $10Dq$ (eV) | 1.2 | 1.2 | 1.2 | 1.3 |
| | $D_t$ (eV) | 0.050 | 0.050 | 0.050 | 0.050 |
| | $D_s$ (eV) | 0.020 | 0.020 | 0.020 | 0.020 |
| LMCT | $EG2$ | −0.7 | −0.7 | −0.5 | −0.6 |
| | $EF2$ | −2.1 | −2.1 | −1.1 | −1.1 |
| | $T_{b_1}$ | 1.5 | 1.5 | 1.5 | 1.5 |
| | $T_{a_1}$ | 1.5 | 1.5 | 1.5 | 1.5 |
| | $T_{b_2}$ | 0.2 | 0.2 | 0.2 | 0.7 |
| | $T_e$ | 0.2 | 0.2 | 0.2 | 0.7 |
| MLCT | $EG3$ | −1.0 | −1.0 | 0.0 | −1.0 |
| | $EF3$ | 0.0 | 0.0 | 1.5 | 0.0 |
| | $T_{b_1}$ | 0.6 | 0.6 | 0.6 | 0.7 |
| | $T_{a_1}$ | 0.6 | 0.6 | 0.6 | 0.7 |
| | $T_{b_2}$ | 1.4 | 1.4 | 1.7 | 1.2 |
| | $T_e$ | 1.4 | 1.4 | 1.2 | 0.6 |
| Configuration | % $\lvert 3d^2\mathrm{L}^-\rangle$ | 12 | 12 | 12 | 7 |
| | % $\lvert 3d^3\rangle$ | 57 | 57 | 57 | 57 |
| | % $\lvert 3d^4\underline{\mathrm{L}}\rangle$ | 31 | 31 | 31 | 36 |
| # holes | | 6.82 | 6.82 | 6.81 | 6.69 |

**Table S.VIII** Ligand Field parameters for $Cr^{IV}$.

| | | 90° incidence 300 V bias | | 90° incidence no bias | 45° incidence no bias |
|---|---|---|---|---|---|
| | | 300 K | 150 K | 150 K | 150 K |
| | $\kappa$ (%) | 90 | 90 | 90 | 90 |
| | $\zeta_{2p}$ (eV) | 5.67 | 5.67 | 5.67 | 5.22 |
| | $\zeta_{3d}$ (eV) | 0.047 | 0.047 | 0.053 | 0.029 |
| | $10Dq$ (eV) | 1.1 | 1.3 | 1.3 | 1.4 |
| | $D_t$ (eV) | 0.020 | 0.150 | −0.020 | −0.020 |
| | $D_s$ (eV) | −0.020 | −0.200 | 0.020 | 0.000 |
| LMCT | $EG2$ | 4.0 | 4.5 | 3.5 | 2.5 |
| | $EF2$ | 3.0 | 3.5 | 3.0 | 1.5 |
| | $T_{b_1}$ | 0.0 | 0.0 | 0.6 | 0.6 |
| | $T_{a_1}$ | 0.5 | 0.8 | 0.6 | 0.6 |
| | $T_{b_2}$ | 1.7 | 2.0 | 0.9 | 0.9 |
| | $T_e$ | 1.3 | 1.0 | 1.1 | 1.1 |
| MLCT | $EG3$ | 0.0 | 0.0 | 0.0 | 0.0 |
| | $EF3$ | 0.0 | 0.0 | 0.0 | 0.0 |
| | $T_{b_1}$ | 0.0 | 0.0 | 0.0 | 0.0 |
| | $T_{a_1}$ | 0.0 | 0.0 | 0.0 | 0.0 |
| | $T_{b_2}$ | 0.0 | 0.0 | 0.0 | 0.0 |
| | $T_e$ | 0.0 | 0.0 | 0.0 | 0.0 |
| Configuration | % $\|3d^1\mathrm{L}^-\rangle$ | 0 | 0 | 0 | 0 |
| | % $\|3d^2\rangle$ | 74 | 81 | 78 | 70 |
| | % $\|3d^3\underline{\mathrm{L}}\rangle$ | 26 | 19 | 22 | 30 |
| # holes | | 7.74 | 7.81 | 7.78 | 7.70 |

## Notes and references


1 S.-I. Ohkoshi, A. Fujishima and K. Hashimoto, *J. Am. Chem. Soc.*, 1998, **120**, 5349–5350.

2 T. Nuida, T. Hozumi, W. Kosaka, S. Sakurai, S. Ikeda, T. Matsuda, H. Tokoro, K. Hashimoto and S.-I. Ohkoshi, *Polyhedron*, 2005, **24**, 2901–2905.

3 E. Coronado, M. Makarewicz, J. P. Prieto-Ruiz, H. Prima-García and F. M. Romero, *Adv. Mater.*, 2011, **23**, 4323–4326.

4 E. Coronado, M. Fitta, J. P. Prieto-Ruiz, H. Prima-García, F. M. Romero and A. Cros, *J. Mater. Chem. C*, 2013, **1**, 6981–6985.

5 I. I. Horcas, R. Fernández, J. M. Gómez-Rodríguez, J. Colchero, J. Gómez-Herrero and A. M. Baró, *Rev. Sci. Instrum.*, 2007, **78**, 013705.

6 S. Nakanishi, G. Lu, H. M. Kothari, E. W. Bohannan and J. A. Switzer, *J. Am. Chem. Soc.*, 2003, **125**, 14998–14999.

7 H. Prima-García, E. Coronado, J. P. Prieto-Ruiz and F. M. Romero, *Nanoscale Research Letters*, 2012, **7**, 232.

8 E. Stavitski and F. M. F. de Groot, *Micron*, 2010, **41**, 687–694.

9 `http://www.anorg.chem.uu.nl/CTM4XAS/index.html`.

10 H. Ogasawara, A. Kotani, K. Okada and B. T. Thole, *Phys. Rev. B*, 1991, **43**, 854–859.

11 H. Ogasawara, A. Kotani, R. Potze, G. A. Sawatzky and B. T. Thole, *Phys. Rev. B*, 1991, **44**, 5465–5469.